VOL. 03 NO. 5,
FEBRUARY, 2024
E-ISSN 3027-1339
P-ISSN 3026-8257

African Scholar Publications & Research International
www.africanscholarpub.com

Journal of Systematic, Evaluation and Diversity Engr. (JSEDE)

Ultrasound Aided Adsorption of Cu (II), Ni (II) and Mn (II) from Wastewater onto Activated Carbon Developed from Melon Husk

[1]Esther Bernard, S.A Eya[2] Abel Adekanmi Adeyi[3] and Abel Inobeme[4]

[1]Department of Chemical Engineering, Nasarawa State University Keffi Nigeria.
[2]Department of Civil Engineering, Nasarawa State University Keffi Nigeria.
[3]Department of Chemical Engineering and Petroleum Engineering, Afe Babalola University Ado-Ekiti (ABUAD), PMB 5454, Ado-Ekiti, Ekiti State, Nigeria.
[4] Department of Chemistry Edo State University Uzairue Nigeria.
estherbernard667@gmail.com

Abstract

The three metal ions Cu (II), Ni (II), and Mn (II) were removed from plating wastewater using activated carbon made from melon husks (ACM), both in the presence and absence of ultrasonic vibrations. The effects of adsorbent dosage, contact time, and pH on the adsorption of Cu (II), Ni (II), and Mn (II) from wastewater were investigated in batch adsorption studies. A comparison of adsorption studies carried out with the aid of ultrasonic waves showed a higher uptake of heavy metal ions in the presence of ultrasonic waves than without ultrasonic vibrations. The adsorption capacity (Qm) of the activated carbon (ACM) obtained from the Langmuir isotherm was higher in the presence of ultrasonic waves. The adsorption capacity (Qm) of ACM in the presence of ultrasonic waves was 2.235 mg/g, 1.473 mg/g, and 0.985 mg/g for Cu (II), Ni (II), and Mn (II); without irradiation, the values were 1.742 mg/g, 0.704 mg/g, and 0.524 mg/g for Cu (II), Ni (II), and Mn (II) by Langmuir isotherm models. The adsorption process was

irradiated with an ultrasonic wave and, without irradiation, obeyed pseudo-second-order kinetics. The adsorbents were characterized using SEM and EDS analyses. The SEM images revealed the porous structure of the adsorbent for the adsorption of Cu (II), Ni (II), and Mn (II).

Keywords: Adsorption Isotherm, activated carbon, melon husk, electroplating wastewater, ultrasonic wave, pseudo- second-order kinetics

Introduction

The environment is exposed to harmful substantial metals by industries such as mining, plating, dyeing, vehicle manufacture, ceramics, metallurgical, and metal processing **(1).** The presence of heavy metals' in the environment has resulted in a slew of environmental issues **(2). Heavy metals are non-biodegradable and can accumulate in living tissues, thereby causing numerous disorders and illnesses(3).** Heavy metals such as copper (Cu^{2+}) as a hazardous metal have been linked to causing neurotoxicity, universally known as "Wilson's disease," in humans. Copper has also been reported to cause jaundice, lung cancer, and an enlarged liver in certain people(4)**. While nickel ion (Ni^{2+}) exposure in the environment above its permissible limit causes skin dermatitis, lung fibrosis, renal oedema, and gastrointestinal distress, among other diseases**(5). Exposure to the manganese ion (Mn) above its permissible limit has detrimental health effects. Excessive manganese ion consumption, most from inhalation or ingestion, can cause central nervous system (CNS) damage as well as renal failure (5).

Owing to the magnitude of problems caused by heavy metal pollution, various orthodox treatment approaches have been established for the treatment of heavy metals in wastewater before they are poured out into the environment(6). orthodox treatment methods such as chemical precipitation(7), electrocoagulation(8), oxidation-reduction(9), ion exchange(10), ultra-filtration(11), flocculation(12), reverse osmosis(13), and membrane separation(14). However, there are some environmental and economic disadvantages associated with the mentioned treatment methods, which include the high costs, delay in operations, inadequate removal effectiveness, production of secondary

pollutants, complex technical treatment, dependence on oxidizing agents, and slow operational duration(15).

On the other hand, the adsorption treatment method has been well-known as an alternative treatment quality method compared to other methods because of its low cost, effectiveness, ease of use, great adaptability, reusability, and availability of different adsorbents (16–18). Much emphasis has been paid to the usage of activated carbon (AC) as an adsorbent in the adsorption process because of its high internal surface area, permeable structure, large surface area, functional surface clusters, and ample adsorption capacity(19). Still, the high cost of production associated with the use of commercial activated carbon for the purposes of water and wastewater treatment has necessitated the research and utilization of affordable, abundantly readily available agricultural waste products for the production of activated carbon. The use of agricultural waste products for activated carbon production converts low-value agricultural waste into valuable, high-use adsorbents. It is also an excellent means of managing agricultural solid waste, reducing environmental pollution, and contributing to the increased economic potential of a country through a decrease in activated carbon importation(20).

In recent times, several agricultural waste products have been employed by researchers for the production of activated carbon. Some of these waste products include corn cobs(21), mango seed coat(22), rice husk(23), mustard husk(24), coconut shell(25), almond shell(26), acorn shell(27), walnut shell(28), sunflower(29), corn bract(30), pecan nutshell(31), peanut shell(32) and orange peel(33).In this study, melon seed husk was used for the preparation of activated carbon.

Melon seed plant belongs to the Cucurbitaceae vegetable family. Cucurbitaceae are a large vegetable family composed of nearly 100 generation and 750s species. This family of plants is famous for its vast genetic diversity(34)**.** This group of plants is noted for its incredible genetic variety and wide range of adaptation, which encompasses tropical and subtropical climates, arid deserts, and temperate climates (35). Egusi (Colocynthis citrullus L.) is a member of the Cucurbitaceae family's Citrullus genus, which includes a vast variety of varieties that are commonly referred to as melons. Egusi is one of the three hundred melon types situated in equatorial Africa, and it is grown for its seeds, which are high in oil (53%) and protein (28%)(36). It is grown in the Middle East and a few other African nations: Nigeria, Ghana, Togo, Benin, and Cameroon(37). In Nigeria, Egusi production has risen to about five

hundred thousand metric tons per year. This may be connected to melon seed oil, which has been used as a feedstock for the manufacturing of biodiesel as well as for use in food, cosmetics, and medicine(38). In Nigeria, the relative increase in the production of vegetable oil and food from melon seeds has generated a substantial amount of waste from melon seeds, known as melon seed husk (MSH). The large amounts of waste generated and littering the environment have necessitated the conversion of MSH into a usable product, such as activated carbon.

ln recent times, the use of activated carbon produced from agricultural waste garbage as an adsorbent for water and wastewater treatment has been employed. Activated carbon has been shown to be a useful adsorbent. Nonetheless, due to its long microporous diffusion path, it requires a possible enhancement technology to aid the adsorption process(18). Ultrasound irradiation has been recognized as a possible improvement in technology to aid the adsorption process (3).

Acoustic cavitation, a phenomenon that causes ultrasound to be irradiated, has been shown to hasten the mass transfer process (39). Cavitation is the rapid formation, expansion, and deflation of bubbles in a brief period of time that produces a considerable quantity of energy in a single location(40). Acoustic cavitation is a sound wave that produces pressure vibrations in the range of 16–100 kHz to provide the necessary cavitation intensity (41). Although it hasn't yet been fully utilized, researchers have reported using ultrasonic cavitation technology for wastewater treatment.

A lot of research work has been carried out previously using activated carbon to take out several heavy metals from simulated wastewater. Although not much work has been reported on the adsorption of metal ions from simulated wastewater enhanced by ultrasound.

However, most of the studies have not considered the influence of ultrasound on the adsorption of competitive metals from wastewater for available space on activated carbon. Thus, the present study focused on how ultrasound affects the adsorption of Cu (II), Ni (II), and Mn (II) from electroplating effluent onto melon husk-based activated carbon.

Materials and Method

Materials

BDH and Burgoyne manufacture analytical-grade potassium chloride (KCl) and hydrochloric acid (HCI), with a purity in percentage ranging from 95 to 99.9%, which were purchased from Panlac, a chemical retailer stores in Niger State, Nigeria.

Samples gathering and preparation

Melon husks were collected from a melon seed milling factory in Kpakungu, Minna, Niger State, Nigeria. To get rid of any unwanted pollutants, the melon husk was cleaned with distilled water and further oven-dried at 105 ºC to get rid of any leftover water. The oven-dried sample was sieved through a 500 μm sieve after size reduction. Prior to pyrolysis, the powdered melon husk sample was submitted to thermogravimetric analysis (TGA) as well as proximal analysis to determine the best temperature for carbonization and activation. The powered melon husk sample was further impregnated with 1.0 M potassium chloride (KCl) for 24 hours and carbonized and activated at 500ºC for 15mins

Proximate analysis

The sample's moisture content was assessed using the thermal drying technique. The procedure was followed in line with ASTM D2867-09. In a washed, dried, and weighed crucible, 1.0 g of the samples was deposited. The crucible was placed in an oven and dried for 1 hour at 105°C. Equation 1.0 was used to calculate the percentage moisture content (percent M.C).

$$M.C = \frac{M_i - M_f}{M_i} \times 100 \qquad 1$$

where M.C stands for the sample's moisture content, Mi for the sample's initial mass (in grams) before heating, and M_f for the sample's final mass (in grams).

The quantity of ash was determined using the ASTM D 2017 standard. 0.3 g of the sample made from melon husk was deposited in a weighed crucible, which was then transferred into a muffle furnace and burned for 1 hour at 760 ºC. The crucible was removed from the muffle furnace and set inside a desiccator to cool to ambient temperature. The sample was evaluated after cooling. Equation 2 was used to obtain the percentage ash content (percent AC).

$$A.C = \frac{W_a}{W_S} \times 100 \qquad 2$$

W_a and W_s stands for mass of ash and sample mass before incineration respectively.

The volatile content of the sample was measured using the standard method ASTM D5832-98.

In a muffle furnace, 1.0g of the sample made from melon husk was burned at 850°C for 10 minutes. The crucible was removed from the muffle furnace and set inside a desiccator to cool to room temperature. Using the crucible's mass and the sample's weight after cooling, equation 3 was employed to evaluate volatile content (VC)

$$V.C = \frac{w_o - w_f}{w_o} \times 100 \quad 3$$

w_o is the initial mass of the sample before incineration and wf is the final mass of the sample after incineration.

The fixed carbon content was implemented in accordance with ASTM D 121 (2001). By deducting 100 from the total of the percentage compositions of moisture, volatile, and ash contents, the fixed carbon content was computed. The carbon content was computed using equation 4.

Fixed carbon (wt%) = 100 − (MC (wt%) + VM (wt%) + Ash (wt%)) 4

Characterization of Samples

For a detailed examination of the samples, different analyses were conducted on the samples using the Fourier transform infrared, thermogravimetric, scanning electron microscopy, and X-ray diffractometer analyzers.

Batch adsorption studies with and without ultrasound

The influence of a few parameters on the uptake of the metal ions (copper, nickel, and manganese) from electroplating wastewater using the newly developed adsorbent from melon husk was examined. The following effects of parameters are taken into account: contact time, adsorbent dosage, and pH. An ultrasonic bath and a water bath shaker were used to perform the adsorption procedure. A 40 kHz-operating ultrasonic bath with the model number SB25-12DT was used.

Influence of contact time

The influence of contact time on the uptake of heavy metal ions was studied for a time frame of 90 minutes. In ten diverse conical flasks holding 50 ml of measured plating wastewater, 0.6g of the developed activated carbon was applied. With the help of a

water bath shaker and an ultrasonic bath, the adsorption process was carried out at a temperature of 30 °C and at various contacting times, which ranged from 15 to 90 min. The contents of each flask were filtered and further examined using an atomic adsorption spectrometer (AAS) at the conclusion of each agitation and irradiation period.

Influence of adsorbent dosage

Five conical flasks containing 50 ml of electroplating wastewater and weighing grams of the developed adsorbents ranging from 0.3 to 1.5 g each were added, corked, and agitated in a shaker at 200 rpm for one hour at 30 °C. Following the agitation phase, the contents of each flask were filtered and subjected to an AAS analysis. The ultrasonic bath was also used to study the effect of dosage. Furthermore, five conical flasks containing 50 ml of electroplating wastewater were corked and subjected to irradiation at a frequency of 40 Hz for 30 min at a temperature of 30 °C with various dosages of the adsorbent ranging from 0.3g to 1.5g. Each flask's contents were filtered before being subjected to additional analysis using an atomic adsorption spectrometer (AAS).

Influence of pH

The influence of pH on the uptake of metal ions was examined in a range of 3.0 to 7.0. The measured electroplating wastewater of 50 ml was divided among five conical flasks with a capacity of 250 ml. With a solution of HCI and NaOH, the pH was raised from 3.0 to 7.0, while the optimal dosage (1.2g) from a prior study was added and swirled at 200 rpm for 1 hour. The solution was filtered using Whatman filter paper and then examined using AAS at the conclusion of the investigations. The ultrasound bath has also been used to study the pH effect, subjected to irradiation at 40 Hz for a period of 30 min at 30 °C.

Data Analysis

The following formulas were used to determine the percentage removal and the amount of heavy metal ions adsorbed at equilibrium:

$$q_e = \frac{v(C_o - C_e)}{m} \qquad 5$$

$$\%R = \frac{(C_o - C_e)}{C_O} \quad 6$$

where C_0 (mg/cm^3) = initial heavy metal ion concentrations qe, (mg/cm^3) = quantity of metal ion uptake; Ce, (mg/cm^3) = equilibrium concentrations of solution (wastewater) present in wastewater; V (cm^3) = volume of wastewater used; and m (g) = adsorbent weight.

lsotherm models for adsoption

The Langmuir(47), Freundlich(48), and Dubinin–Radushkevich(49) Models were engaged to explain and study the mechanics of the adsorption of metal ions on the developed adsorbent. Equation 7 mathematically expresses the Langmuir isotherm mode.

$$\frac{C_e}{q_e} = \frac{1}{K_L q_m} + \frac{C_e}{q_m} \quad 7$$

The Freundlich model is illustrated by equation 8

$$\ln q_e = \ln K_F + \frac{1}{n_F} \ln C_e \quad 8$$

Models such as Dubinin-Radushkevich are one more empirical model that was initiated for the adsorption course based on pore filling. The adsorption process on both homogeneous and heterogeneous surfaces is frequently described in this way.

$$\ln q_e = \ln q_s - \ln k_{ad} \varepsilon^2 \quad 9$$

Ce(mg/L) = equilibrium concentration of heavy metal ions in wastewater from electroplating; qe(mg/g) = heavy metal ions adsorbed amount at equilibrium; and qm(mg/g) = the highest quantity of heavy metal ions that can be absorbed per weight of the adsorbent, KF and nF relate to Freundlich adsorption capacity and intensity, respectively. Qs (mg/g) and Kad (mol^2 /kJ^2) are D-R isotherm model constants that relate to adsorption capacity and adsorption mean free energy and are also known as Polanyi potential parameters. KL (L/mg) = the equilibrium constant for the Langmuir model.

Adsorption kinetic models

Employing kinetic models such as the pseudo-first-order(50), pseudo-second-order(51), Elovich (52) and intraparticle diffusion(53), it was possible to study the mechanism of Cu (II), Ni (II), and Mn (II) adsorption onto ACM

Equation 10, represents the expression for the pseudo-first-order rate concept.

$$\ln(q_e - q_t) = \ln(q_e - k_1 t) \quad 10$$

Equation 11, represent pseudo-second-order concept.

$$\frac{t}{q_t} = \frac{1}{k_2 q_e^{\,2}} + \frac{t}{q_e} \quad 11$$

Equation 12, is used to express the intraparticle diffusion concept.

$$q_t = k_i t^{0.5} + C \quad 12$$

Equation 13, is used to express the Elovich concept

$$q_t = \frac{1}{\beta} In(\alpha\beta) + \frac{1}{\beta} Int \quad 13$$

qt (mg/g) = the number of heavy metal ions that were adsorbed at time t. (min), qe (mg/g) = the equilibrium amount of heavy metal ions adsorbed, and k1 (min-1) and k2 (mg/g.min) = pseudo-first-order and pseudo-second-order rate constants, respectively, C (mg/g) = intercept from the plot of qt against $t^{0.5}$, and ki (mg/g.$min^{0.5}$) and α (mg/g.min) = the intraparticle diffusion and Elovich rate constants, respectively. Meanwhile, β (mg/g.min) = Elovich's parameter related to the extent of adsorbent surface coverage and energy of chemisorption.

Results and Discussion

Proximate analysis of melon husk

The proximate analysis of a melon husk sample, as represented in Table 1, revealed a fixed carbon content of 40.51%, a low moisture content of 1.0%, and a low ash level of 9.00%, indicating that the material is rich in organic matter and could be used to make activated carbon(55).

Table 1: Proximate properties of melon husk

S/n	Temperature (°C)	Time (min)	Moisture content (%)	Volatile content (%)	Ash content (%)	Fixed content (%)
1.0	500	15	1.00	49.49	9.00	40.51

Characterization of Melon husk(MH) and Activated carbon(ACM)

Analysis using Thermogravimetric Analyzer (TGA)

Figure 1 displays the results of the thermogravimetric analysis (TGA) of the melon husk sample, which showed three distinct stages of breakdown. The first stage (below 200°C) is the drying phase, when moisture is largely discharged across the region. Figure 1 demonstrates that the first stage of decomposition takes place between 25.11 and 153.02 °C, which corresponds to a weight loss of 5.28 percent brought on by the moisture being drawn out of the sample of melon seed husk.

The removal of volatiles (devolatization) occurs in the second stage, which is an exothermic reaction involving hemicellulosis and cellulose, as well as a small amount of lignin, which is a crucial step in the waste-to-carbon conversion process. At this point, a significant amount of weight loss has occurred

It's also known as the active pyrolysis region (Saffe et al., 2014). As indicated in Figure 1, the degradation temperature range for the melon seed husk sample was 153.02-300.23 °C, with a weight loss of 59.01%. This implies the elimination of volatile matters(38).

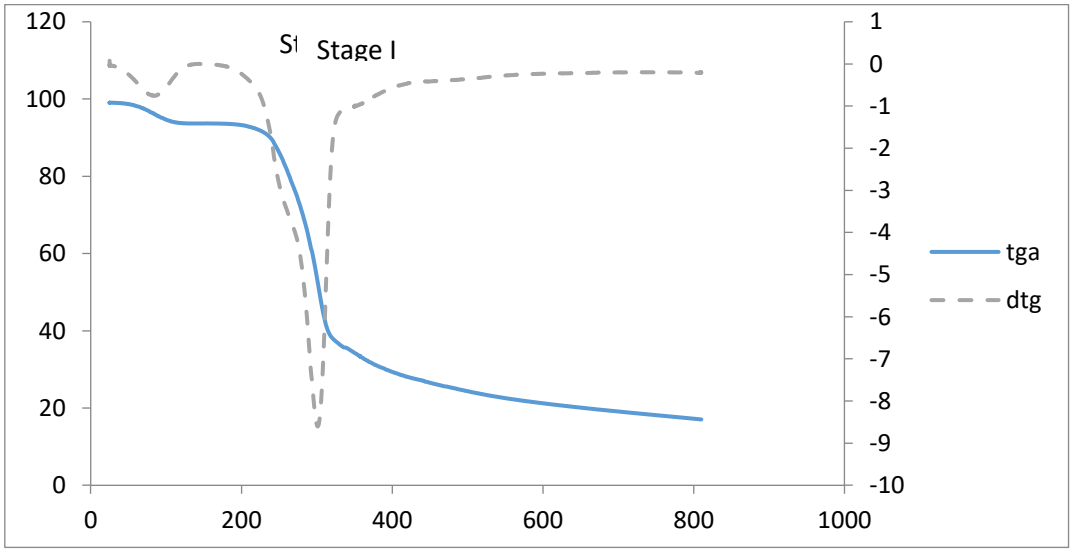


Figure 1:TGA/DTG of melon husk

Surface area and pore size

The Dubinin-Radushkevich technique was employed for the investigation of the surface area of developed activated carbon made from melon husk and raw melon husk, as evident in Table 2.

Table 2: Surface area and typical pore size of raw husk of melon sample and developed activated carbon from husk of melon

Sample	S_{BET}	Pore volume	Pore size
	(m^2/g)	cm^3/g	nm
Raw melon husk	301.4550	0.1227	2.9520
Carbonized sample from Melon	356.9150	0.1497	2.7960
Activated carbon from melon husk (ACM)	1285.7510	0.4646	3.1910

The developed activated carbon showed the highest surface area of 1285.7510 m^2/g due to impregnation and activation with potassium chloride, leading to the development of more pores and the extraction of disordered carbon(56) The carbonized sample with a surface area of 356.9150 m2/g, which is slightly higher than the surface area of the raw melon husk with a surface area of 301.4550 m2/g, could be the result of heating during carbonization.

Analysis of X-ray diffraction (XRD)

For characterizing the structure of the adsorbents, X-ray diffraction (XRD) was used. Melon husk, char made from the raw husk, and the developed activated carbons were all examined
using XRD.

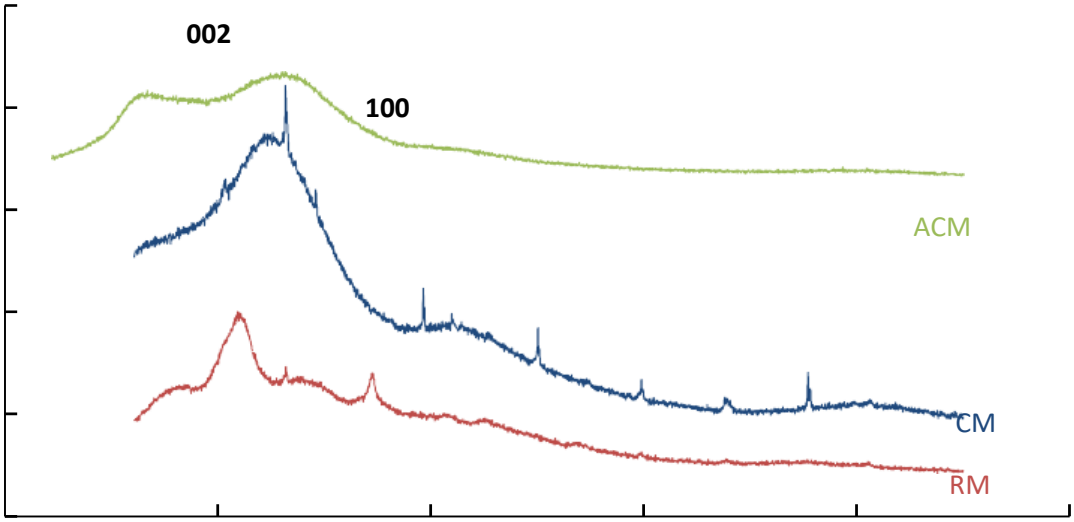


Figure 2; XRD of melon husk (RM) Char (CM) and activated carbon(ACM)

Figure 2 depicts the X-ray diffraction patterns of raw melon husk and char-made and developed activated carbon. The (002) plane and (100) plane, respectively, are credited with peaks of 2 θ = 21.916° and 2 θ = 42.875°, respectively, meant for the X-ray diffraction of melon husk, while the (002) plane and (100) plane are attributed to the peaks at 2 θ = 26.375° and 2 θ = 41.743°, respectively, for the char sample derived from melon husk. The (002) and (100) planes are ascribed to the peaks for activated carbon at 2 θ = 24.978° and 2 θ = 41.478°, respectively. The presence of a significant peak in activated carbon (ACM) at around 2 θ =24.978° (002 planes) indicated that the substance was amorphous in nature. The parameters extrapolated from the diffraction peaks are listed in Table 3.

Table 3: X-ray diffraction characteristics from activated carbon, Char sample and melon husk

Sample	2θ002 (deg)	2θ100 (deg)	d_{002}/nm	d_{100}/nm	crystalline height (Lc)/nm	crystalline width (La)/nm
Melon husk	21.916	42.875	0.405	0.218	3.284	4.650
Char	26.375	41.743	0.338	0.216	1.342	1.004
Activated Carbon	24.978	41.478	0.356	0.218	1.486	0.734

Using the Debyne-Scherrer equation, represented by equation 18, the crystallite sizes of melon husk, char made from melon husk, and activated carbon generated were computed.

$$D = \frac{K\lambda}{\beta \cos} \qquad 14$$

where D (nm) represents the average crystallite size, K stands for the Scherrer crystallite factor, which ranges from 0.2 to 2.0 (0.94 for cubic structures), λ (nm) points to the X-ray wavelength (0.154 nm), β (radians) is the full width at half maximum (FWHM) of the diffraction peak in the XRD pattern, and θ (deg) is the calculated diffraction angle. The calculated crystalline size (La) of raw melon husk was 4.6498 nm, while the calculated activated carbon crystalline size was 0.7340nm. The decrease

in crystalline size apparent in the activated material may be credited to internal structure disorder, which gives rise to a larger specific surface area (33).

SEM analysis

Using a scanning electron microscope, the morphology and surface characteristics of the adsorbent were examined for raw melon husk, char produced, and developed activated carbon, as illustrated in Figure 3(a–c). The pores on the raw melon husk were not obviously visible in Figure 3a, while Figure 3b shows the char produced.

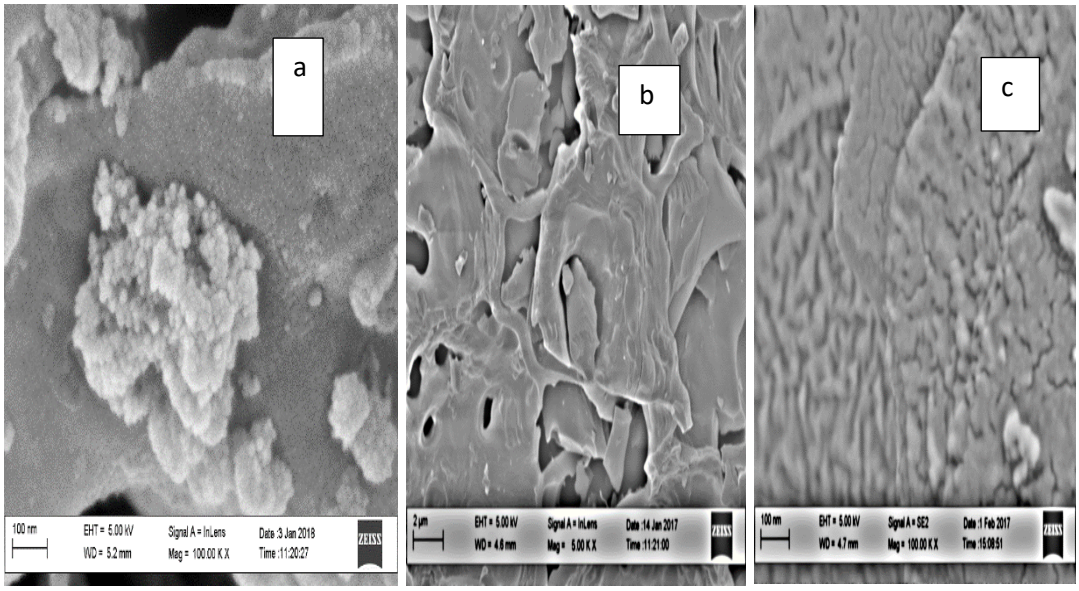


Figure 3(c) :SEM image of raw melon husk(a) char(b) and activated carbon(c)

The char sample derived from melon husk revealed more developed pores than the raw husk, as seen on the SEM. This could be attributed to the removal of volatile matter contents during carbonization. The SEM micrograph of activated carbon developed revealed additional holes, as evident in Figure 3(c), in both the raw and char samples as a result of activation with potassium chloride (KCI). The KCI-carbon connection is increased by activation, which also stimulates KCI molecules to diffuse into pores, increasing the number of pores in the activated carbon.

FTIR analysis

The spectrum analyses were carried out to highlight the active surface functional groups that serve as metal ion binding sites, as made known in Figure 4.

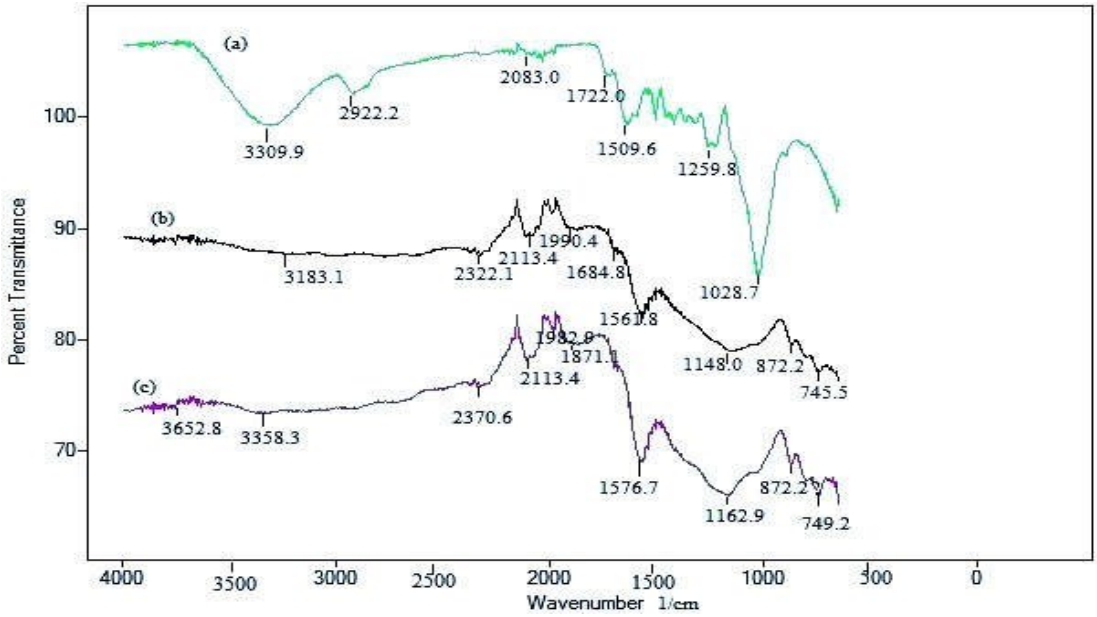


Figure 4: FTIR spectra of melon husk(a), activated carbon produced(b) and metal ions load activated carbon(c)

FTIR spectra of melon husk revealed a substantial wide band at 3309.9 cm-^{1} between 3000 and 3500 cm-^{1}, which points to the existence of free and intermolecular -OH groups(57). C-H and C-C stretch correspond to peaks at 2922.2 and 2083.0 cm-^{1} respectively(58), while the carboxylic acid's C=O stretch and the aromatic ring of lignin's C=C stretch, correspond to peaks at 1722.0 and 1509.6 cm^{-1}(59). Activated carbon FTIR spectra (b) revealed a lower intensity O-H stretching band at 3183.1 cm-^{1} as a result of phenolic groups being broken down and the melon husk structure being dried during activation(59).

Thermal decomposition caused the peaks at 2922.2, 1722.0, and 1259.8 cm^{-1} in raw melon husk to disappear and caused the presence of new weak peaks at 2322.1 and 1684.8 cm-^{1} which were attributed to the C≡Cstretch of alkynes and the -C=C- stretching vibrations in alkenes correspondingly in FTIR spectra (b) which was all as a result of activation(60).

On the activated carbon FTIR spectra (c) loaded with heavy metals, the O-H stretching band at 3183.1 cm^{-1} on FTIR spectra (b) was moved to 3358.3 cm^{-1} due to adsorption, and the emergence of a new band at 3652. 8 cm-^{1} was seen, similar to this, the peaks of activated carbon's FTIR spectra(b) at 2322.1, 1561.8, and 1148.0 cm-1 were relocated to 2370.6, 1576.7, and 1162.9 cm-1, respectively (c) after adsorption.

Experimental Results on Adsorption of heavy metals influence of contact time

Figures 5a and 5b depict the effects of contact time on heavy metal adsorption with ultrasound assistance and adsorption without ultrasound (b), respectively. For both metal ion adsorptions assisted by ultrasound and adsorption without ultrasound, the impact of time was investigated over a period of 15 to 90 min. Figure 5a demonstrates that more metal ions were adsorbed on ACM in the presence of ultrasonic waves than there were when there weren't any ultrasonic waves, as evident in Figure 5b.

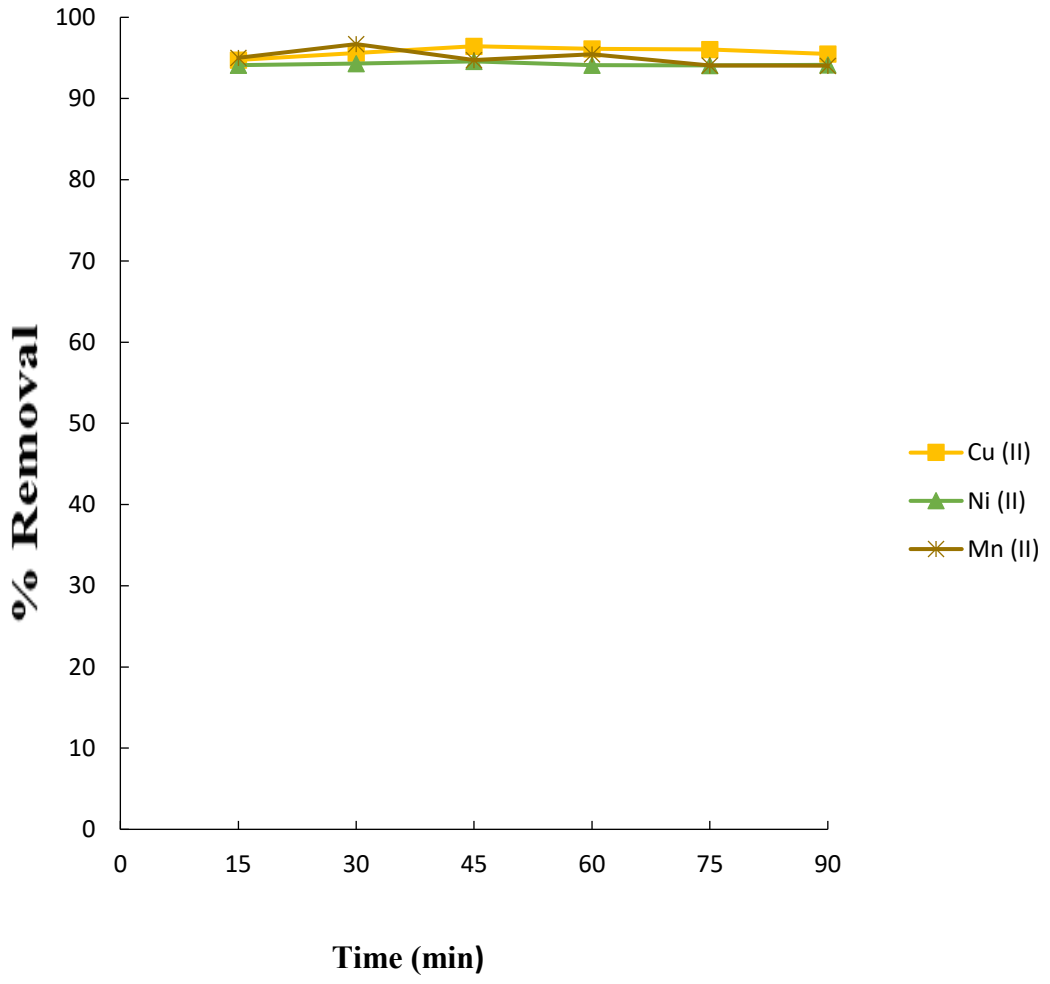


Figure 5a: The influence of time on adsorption of metal ions onto developed activated carbon irradiated at 40Hz

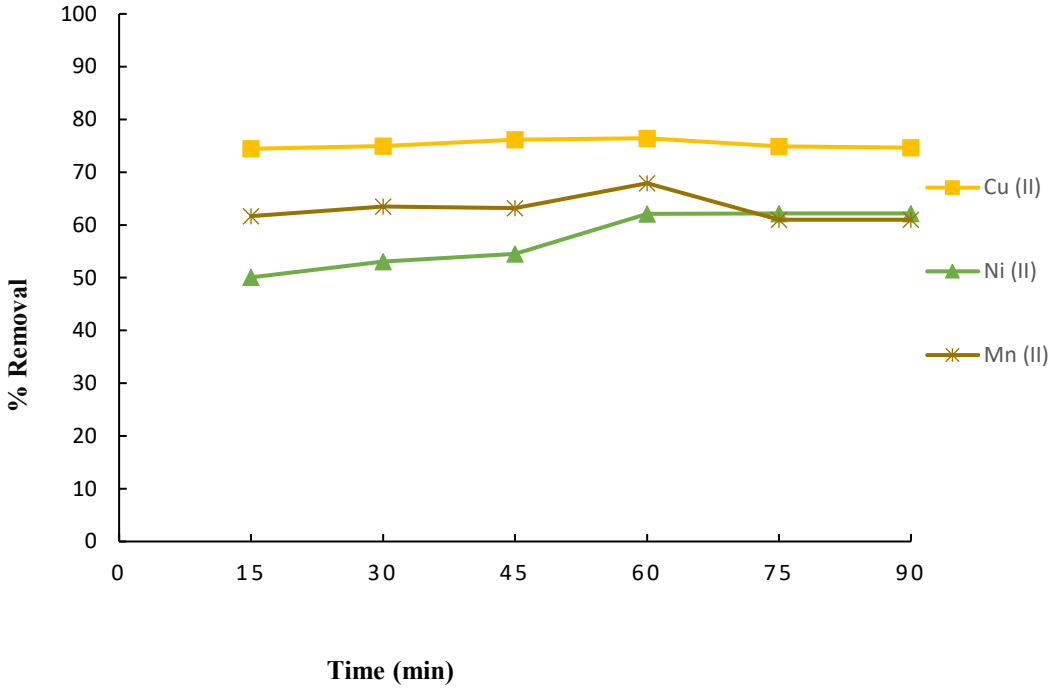


Figure 5b: The influence of time on adsorption of metal ions onto developed activated carbon at 200 rpm

For metal ions aided by ultrasound adsorbed on ACM, it showed rapid removal of metal ions and achieved equilibrium within 30 minutes after the removal of 95.62% Cu (II), 94.32% Ni (II), and 96.70% Mn (II). Having a pattern of Mn^{2+}>Cu^{2+}>$Ni^{2+,}$ whereby the metal ions' ion properties may be responsible for While the removal of heavy metals in the absence of ultrasound achieves equilibrium within 60 minutes for the metal ions, Cu (II), Ni (II), and Mn (II) recorded 75.78%, 40.99%, and 69.99% removal, respectively. Having a trend of $Cu^{2+} > Mn^{2+} > Ni^{2+}$ Metal ions were removed from wastewater more quickly by ACM influenced by an ultrasound pulse due to the cavitation and acoustic streaming processes, which enhanced mass transfer and increased the adsorption rate(61). Rapid adsorption was also seen in the first 30 minutes of sonication. This was credited to the external diffusion of metal ions and the enormous number of accessible adsorption sites at that time (62). Under the influence

of an ultrasonic wave, the optimum time for adsorption of all metal ions on ACM was 30 minutes, which was employed for further research.

Influence of adsorbent dosage

As shown in Figure 6(c) and (d), the impact of adsorbent dosage on the removal of heavy metal ions from ACM after exposure to ultrasonic waves and adsorption in the absence of ultrasound (d) was studied in a range of 0.3g-1.5g.

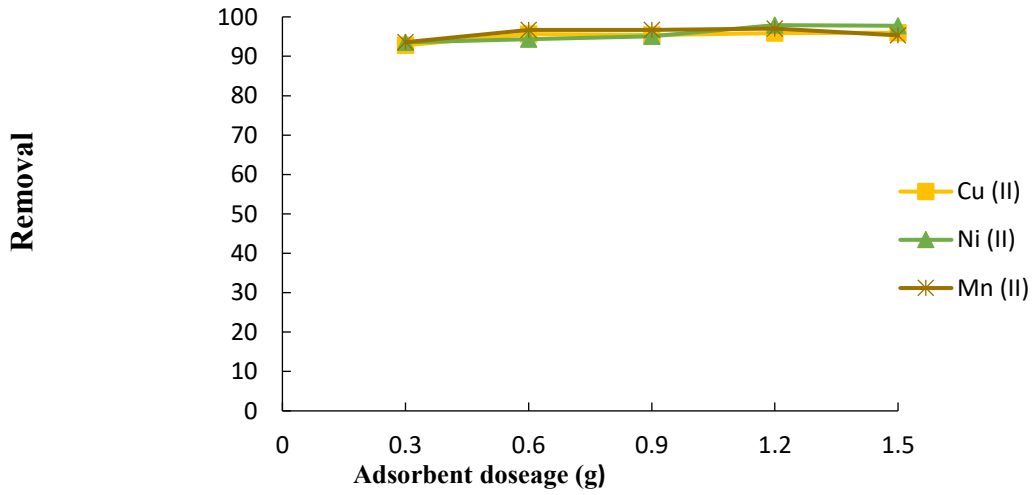


Figure 6(c): The influence of adsorbent dosage on adsorption of metal ions onto developed activated carbon irradiated at 40Hz

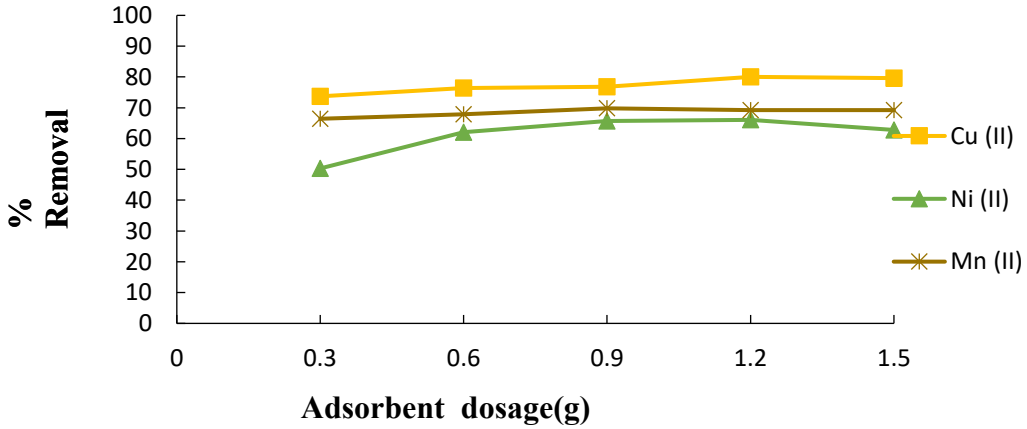


Figure (6d): The influence of adsorbent dosage on adsorption of metal ions onto developed activated carbon agitated at 200rpm

As evident from Figures 6(c) and (d), as the amount of adsorbent dosage increased from 0.3g to 1.5 g, the percentage removal of metal ions increased. The amount of metal ion adsorption on ACM irradiated by ultrasonic wave demonstrated an increase in percentage removal, of which Cu (II) increased from 92.81 to 95.98%, Ni (II) from 93.55 to 97.79%, and Mn (II) from 93.59 to 95.29%, while for adsorption in the absence of ultrasound, Cu (II) increased from 73.72 to 79.67%, Ni (II) from 50.30 to 62.80%, and Mn (II) from 66.44 to 69.23% as the amount of adsorbent dosage increased from 0.3g to 1.5g. There were more binding sites available at greater adsorbent dosages, which led to an increase in the absorption of heavy metal ions (28). Though the increased absorption of heavy metal ions in the presence of ultrasonic waves was primarily caused by the cavitation mechanism (3).

Influence of pH

At pH values ranging from 3.0 to 7.0, the impact of pH on the adsorption of heavy metal ions onto ACM was examined. Figures 7(e) and (f) illustrate the impact of pH on the adsorption of heavy metal ions on ACM exposed to ultrasonic waves and adsorption in the absence of ultrasonic waves.

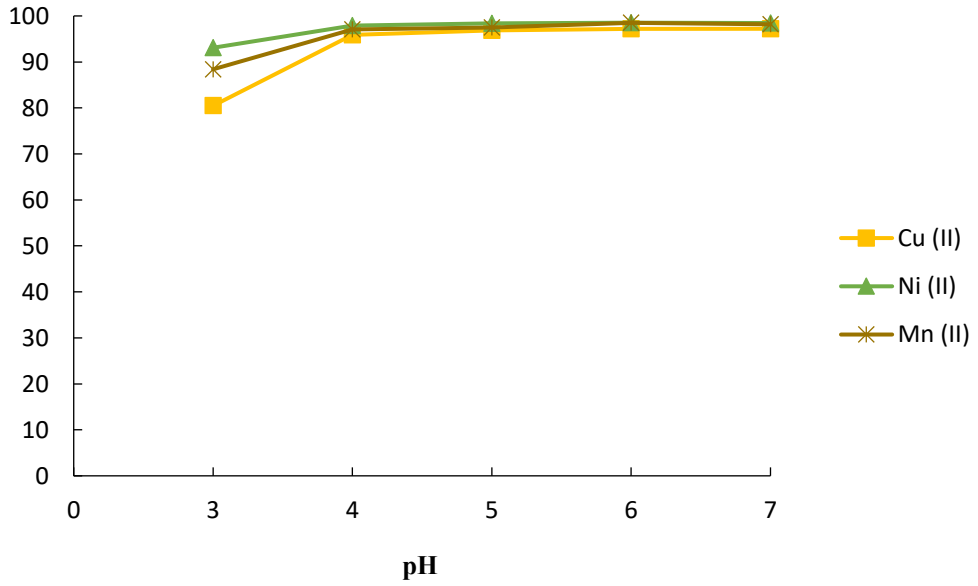


Figure 7(e): The influence of pH on adsorption of metal ions onto developed activated carbon irradiated at 40Hz

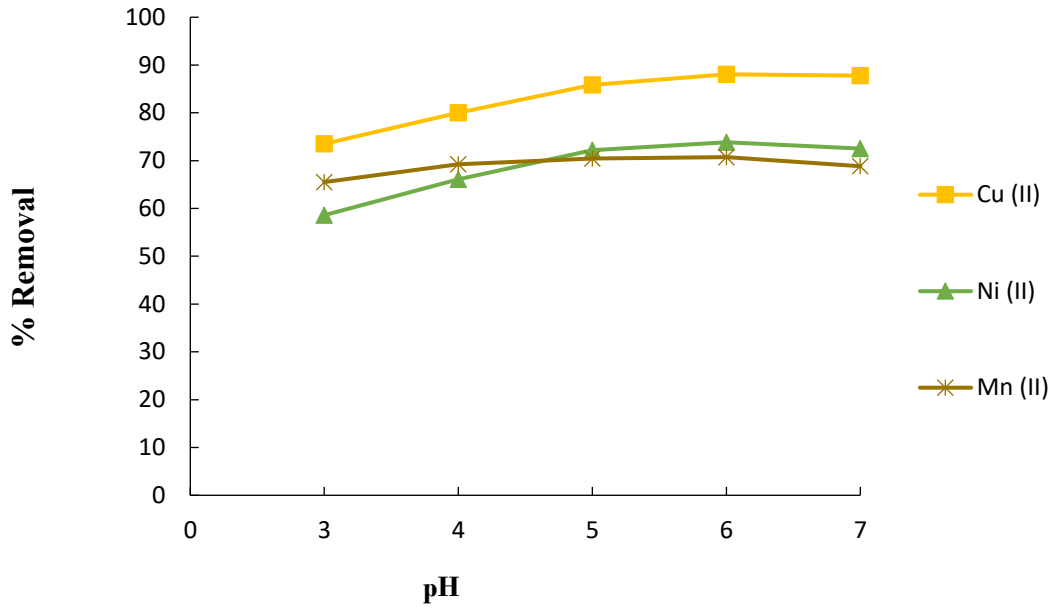


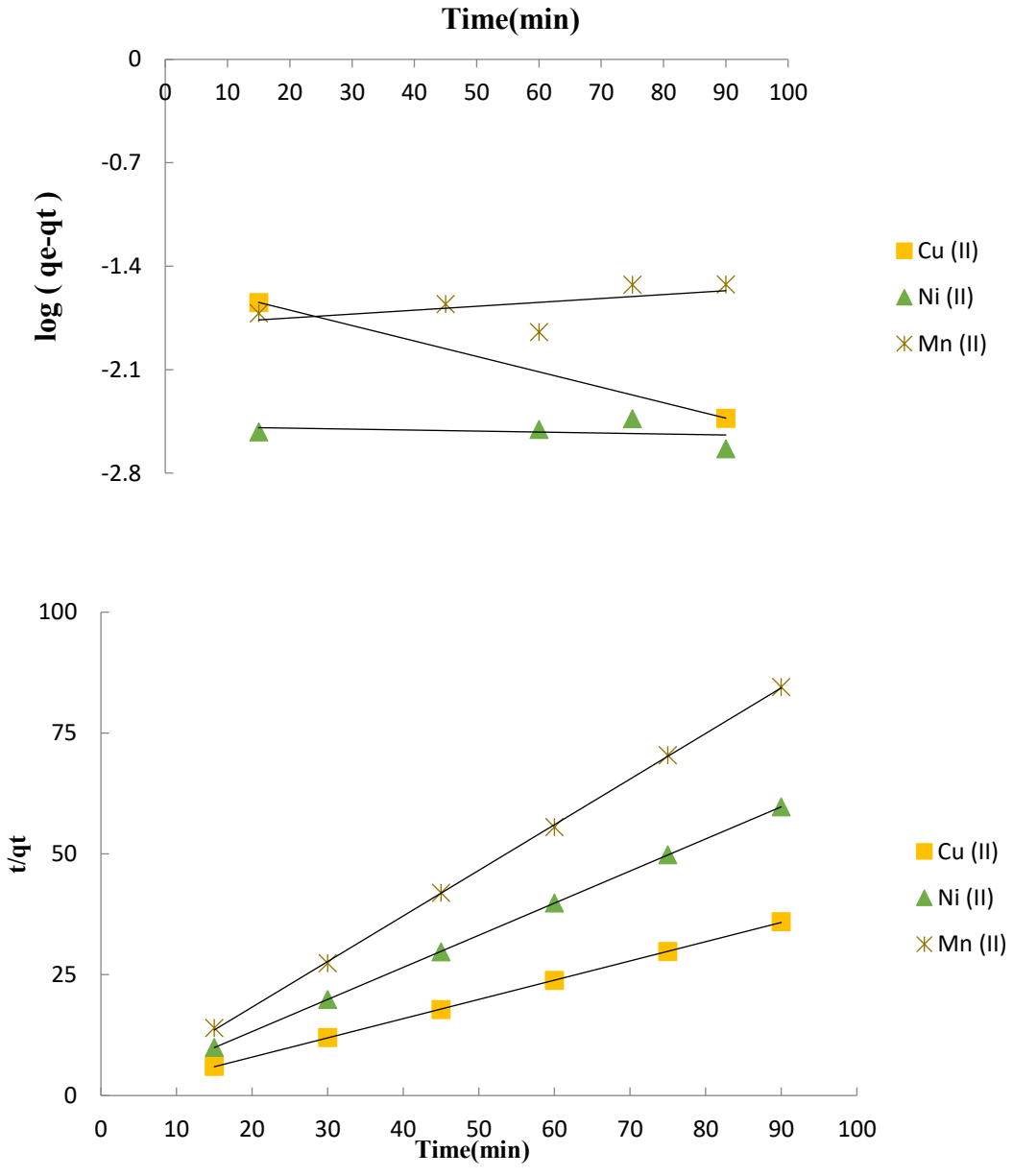
Figure 7(f): The influence of pH on adsorption of metal ions onto developed activated carbon agitated at 200rpm

As the pH of the solution was raised, more heavy metal ions adhered to the ACM. In comparison to the adsorption in the absence of ultrasonic waves, the effect of pH on the adsorption of heavy metal ions subjected to ultrasonic waves was larger. Heavy metal ions subjected to ultrasonic waves at pH 6 had the highest removal rates of Cu (II), Ni (II), and Mn (II), with removal rates of 97.19%, 98.53%, and 98.50%, respectively. While for the same three metal ions, the greatest adsorption occurred at pH 6 in the absence of an ultrasonic wave, of which Cu (II) removal was 88.06%, Ni (II) removal was 73.84%, and Mn (II) removal was 70.73%. Given that the adsorbent surface is deprotonated and negatively charged at higher pH levels, which attract positively charged metal cations, the increase in the percentage of heavy metal ion removal may be explained (63).

Adsorption Kinetics

Using the pseudo-first order, pseudo-second order, Elovich, and intraparticle diffusion models, the kinectics of the adsorption process aided with ultrasonic waves which had higher adsorption rates for metal ions were investigated; the plots are presented in Figure 8(i)-(I). Table 4 displays the values of the computed kinetic parameters

determined for the four kinetic models. Given the higher correlation values (R^2) obtained with the pseudo-second-order model, as apparent in Table 4, the adsorption of heavy metal ions is presumed to follow the model. Additionally, a high agreement between the predicted (qe, cal) and experimental (qe, exp) adsorption capacities demonstrated the pseudo-second-order kinetic model's greatest fitness. The pseudo-second-order kinetics, which best describes uptakes of metal ions, is founded on the hypothesis that the rate-limiting step in this process can be chemisorption.



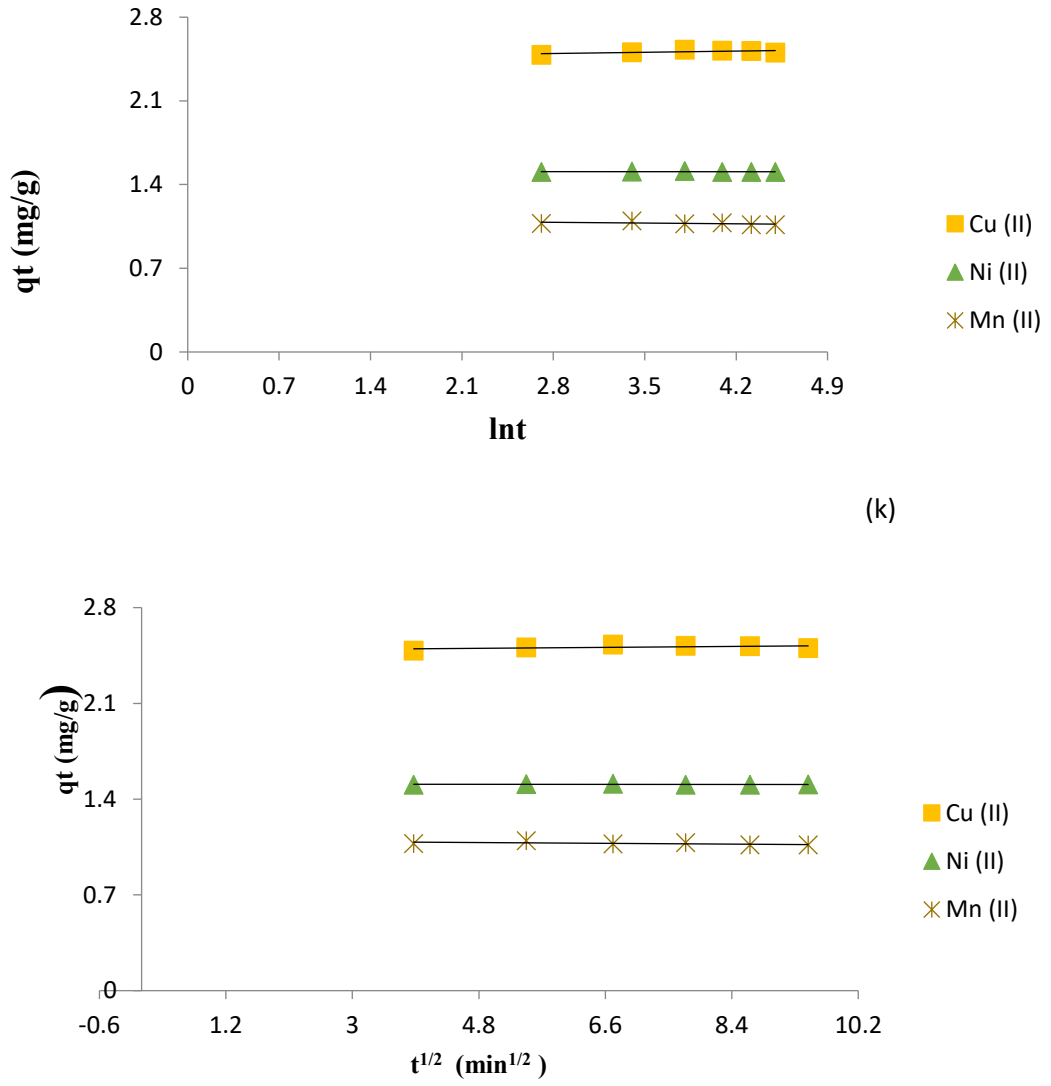


Figure 8(i-l): Pseudo-first-order(i) Pseudo-second-order(j) Elovich,(k) and intraparticle diffusion model(l) of adsorbed metal ions.

Table 4: Kinetic parameters consist of metal ions removed onto developed adsorbent

Metal ions	Pseudo 1st order model				Pseudo 2nd order model					Intraparticle diffusion model	Elovich model
	q_e exp (mg/g)	qe cal mg/g)	R^2	K_1	q_e exp (mg/g)	qe cal mg/g)	R^2	K_2	K_2	R^2	R^2

Cu(II)	2.01	0.07	0.01	2.67	2.01	1.97	1.00	1.59	0.03	0.01	0.08
Ni(II)	0.99	0.12	0.52	2.17	0.99	0.63	0.94	0.18	0.18	0.03	0.12
Mn(II)	0.77	0.05	0.34	2.95	0.77	0.70	0.99	0.10	0.01	-	0.01

Conclusion

A low-cost waste product from melon husk was used to develop activated carbon and successfully applied to remove Cu (II), Ni(II), and Mn (II) ion from plating wastewater. Adsorption studies carried out with the aid of ultrasonic waves showed a higher uptake of heavy metal ions than without ultrasonic waves. Shorter time of 30 min was required in presence of ultrasound for optimum removal of metal ions compared to 60 min and 75 min in the absence of ultrasound. Furthermore, the kinetic data obtained both in the presence and absence of ultrasound were better fitted to the pseudo-second-order kinetic model than the pseudo-first-order model, intraparticle diffusion and Elovich kinetic models. Also the Langmuir model describes satisfactorily the adsorption of metal ions on activated carbon.

In conclusion, a combination of ultrasound with adsorbent materials has exhibited excellent performance to remove heavy metals from electroplating wastewater, and this process is eco- friendly and economical.

REFERENCES

Ali H, Khan E, Ilahi I. Environmental chemistry and ecotoxicology of hazardous heavy metals: Environmental persistence, toxicity, and bioaccumulation. J Chem. 2019;2019(Cd).

Mansourri G, Madani M. Examination of the Level of Heavy Metals in Wastewater of Bandar Abbas Wastewater Treatment Plant. Open J Ecol. 2016;06(02):55–61.

Khaligh A, Zavvar H, Rashidi A. Journal of Applied Chemistry Ultrasonic assisted removal of Ni (II) and Co (II) ions from aqueous solutions by carboxylated nanoporous graphene. J Appl Chem. 2017;11(41):49–58.

Thakur LS. Heavy metal Cu , Ni and Zn : Toxicity , health hazards and their removal techniques by low cost adsorbents : A short overview TECHNIQUES BY LOW COST ADSORBENTS : A SHORT OVERVIEW. Int J plant, Anim Enviromental Sci. 2015;145–157(January).

Ahmed A, Ali A, Hosny A. Adsorption Separation of Nickel from Wastewater by using Olive Stones. Adv J Chem A. 2019;2(1):79–93.

Akpomie KG, Dawodu FA, Adebowale KO. Mechanism on the sorption of heavy metals from binary-solution by a low cost montmorillonite and its desorption potential. Alexandria Eng J. 2015;54(3):757–67.

Jumina, Priastomo Y, Setiawan HR, Mutmainah, Kurniawan YS, Ohto K. Simultaneous removal of lead(II), chromium(III), and copper(II) heavy metal ions through an adsorption process using C-phenylcalix[4]pyrogallolarene material. J Environ Chem Eng [Internet]. 2020;8(4):103971. Available from: https://doi.org/10.1016/j.jece.2020.103971

Qasem NAA, Mohammed RH, Lawal DU. Removal of heavy metal ions from wastewater: a

comprehensive and critical review. npj Clean Water [Internet]. 2021;4(1):0–15. Available from: http://dx.doi.org/10.1038/s41545-021-00127-0
Sai Krishna YVS, Sandhya G, Ravichandra Babu R. Removal of heavy metals Pb(II), Cd(II) and Cu(II) from waste waters using synthesized chromium doped nickel oxide nano particles. Bull Chem Soc Ethiop. 2018;32(2):225–38.
Mishra J, Saini R, Singh D. Review paper on removal of heavy metal ions from industrial waste water effluent. IOP Conf Ser Mater Sci Eng. 2021;1168(1):012027.
Shafiq M, Alazba AA, Amin MT. Removal of heavy metals from wastewater using date palm as a biosorbent: A comparative review. Sains Malaysiana. 2018;47(1):35–49.
Suresh A, Grygolowicz-Pawlak E, Pathak S, Poh LS, Abdul Majid M bin, Dominiak D, et al. Understanding and optimization of the flocculation process in biological wastewater treatment processes: A review. Chemosphere. 2018;210:401–16.
Vidu R, Matei E, Predescu AM, Alhalaili B, Pantilimon C, Tarcea C, et al. Removal of heavy metals from wastewaters: A challenge from current treatment methods to nanotechnology applications. Toxics. 2020;8(4):1–37.
Matsuura KCKT, Ethylenediamine EDA. Removal of heavy metals and pollutants by membrane adsorption techniques. Appl Water Sci [Internet]. 2018; Available from: https://doi.org/10.1007/s13201-018-0661-6
Abdullah N, Yusof N, Lau WJ, Jaafar J, Ismail AF. Recent trends of heavy metal removal from water/wastewater by membrane technologies. J Ind Eng Chem [Internet]. 2019;76(April):17–38. Available from: https://doi.org/10.1016/j.jiec.2019.03.029
Jumina, Priastomo Y, Setiawan HR, Mutmainah, Kurniawan YS, Ohto K. Simultaneous removal of lead(II), chromium(III), and copper(II) heavy metal ions through an adsorption process using C-phenylcalix[4]pyrogallolarene material. J Environ Chem Eng. 2020;8(4):103971.
Kluczka J, Pudło W, Krukiewicz K. Boron adsorption removal by commercial and modified activated carbons. Chem Eng Res Des. 2019;147:30–42.
Bernard E. Equilibrium and Kinetic of Ultrasound-Assisted Adsorption of Chromium (VI) ion from Electroplating Wastewater Using Melon Seed Husk Activated carbon. Jounal turkisH Chem Soc B. 2021;4(2):35–46.
Kluczka J, Pudło W, Krukiewicz K. Boron adsorption removal by commercial and modified activated carbons. Chem Eng Res Des [Internet]. 2019;147:30–42. Available from: https://doi.org/10.1016/j.cherd.2019.04.021
Reza MS, Yun CS, Afroze S, Radenahmad N, Bakar MSA, Saidur R, et al. Preparation of activated carbon from biomass and its' applications in water and gas purification, a review. Arab J Basic Appl Sci [Internet]. 2020;27(1):208–38. Available from: https://doi.org/10.1080/25765299.2020.1766799
Armonio JVM, Caragdag IJ, Escorpizo JA, Miranda KM, Raymundo AJ, Roque E. Production of activated carbon from corn cobs and mango kernels via H 3 PO 4 activation and mediated hydrothermal treatment . MATEC Web Conf. 2019;268:06020.
Kwaghger a, Adejoh E. Optimization of conditions for the preparation of activated carbon from mango nuts using ZnCl 2. Carbon N Y. 2012;1(May):1–7.
Saad MJ, Hua CC, Misran S, Zakaria S, Sajab MS, Abdul Rahman MH. Rice husk activated carbon with naoh activation: Physical and chemical properties. Sains Malaysiana. 2020;49(9):2261–7.
Charola S, Patel H, Chandna S, Maiti S. Optimization to prepare porous carbon from mustard husk using response surface methodology adopted with central composite design. J Clean Prod [Internet]. 2019;223:969–79. Available from: https://doi.org/10.1016/j.jclepro.2019.03.169
Islam MA, Ahmed MJ, Khanday WA, Asif M, Hameed BH. Mesoporous activated coconut shell-derived hydrochar prepared via hydrothermal carbonization-NaOH activation for methylene blue adsorption. J Environ Manage [Internet]. 2017;203:237–44. Available from: http://dx.doi.org/10.1016/j.jenvman.2017.07.029
Zbair M, Ahsaine HA, Anfar Z. Porous carbon by microwave assisted pyrolysis: An effective and low-cost adsorbent for sulfamethoxazole adsorption and optimization using response surface methodology. J Clean Prod [Internet]. 2018; Available from:

https://doi.org/10.1016/j.jclepro.2018.08.155
Altıntıg E, Altundag H, Tuzen M, Sarı A, Sarı A. Effective removal of methylene blue from aqueous solutions using magnetic loaded activated carbon as novel adsorbent. Chem Eng Res Des. 2017;122:151–63.
Miyah Y, Lahrichi A, Idrissi M, Khalil A, Zerrouq F. Adsorption of methylene blue dye from aqueous solutions onto walnut shells powder: Equilibrium and kinetic studies. Surfaces and Interfaces [Internet]. 2018;11:74–81. Available from: https://doi.org/10.1016/j.surfin.2018.03.006
Moralı U, Demiral H, Şensöz S. Optimization of activated carbon production from sunflower seed extracted meal: Taguchi design of experiment approach and analysis of variance. J Clean Prod. 2018;189:602–11.
Lin G, Wang S, Zhang L, Hu T, Peng J, Cheng S, et al. Synthesis and evaluation of thiosemicarbazide functionalized corn bract for selective and efficient adsorption of Au(III) from aqueous solutions. J Mol Liq. 2018;258(Iii):235–43.
Lima HHC, Maniezzo RS, Llop MEG, Kupfer VL, Arroyo PA, Guilherme MR, et al. Synthesis and characterization of pecan nutshell-based adsorbent with high specific area and high methylene blue adsorption capacity. J Mol Liq [Internet]. 2019;276:570–6. Available from: https://doi.org/10.1016/j.molliq.2018.12.010
Cai W, Li Z, Wei J, Liu Y. Synthesis of peanut shell based magnetic activated carbon with excellent adsorption performance towards electroplating wastewater. Chem Eng Res Des [Internet]. 2018;140:23–32. Available from: https://doi.org/10.1016/j.cherd.2018.10.008
Xie Z, Guan W, Ji F, Song Z, Zhao Y. Production of biologically activated carbon from orange peel and landfill leachate subsequent treatment technology. J Chem. 2014;2014(6).
Velkov N, Petkova V. Crops from Cucurbitaceae in collection of the Maritsa Vegetable Crops Research Institute, Plovdiv - local cultivars and their application in breeding programme. Agric Sci Technol [Internet]. 2014;6(2):134–42. Available from: http://agriscitech.eu/wp-content/uploads/2014/06/003.pdf
Giwa SO, Chuah LA, Adam NM. Fuel properties and rheological behavior of biodiesel from egusi (Colocynthis citrullus L.) seed kernel oil. Fuel Process Technol [Internet]. 2014;122:42–8. Available from: http://dx.doi.org/10.1016/j.fuproc.2014.01.014
Citrullus L, I AAI, Aa W. Estimation of Some Anti-nutritional Factors in Oil-Free Seed Cake of Egusi. Res Rev J Food Dairy Technol. 2014;2(1):9–11.
Lawal SS, Olalekan RI. Physicochemical properties of Citrullus lanatus (Melon Seed) and Cocos nucifera (Coconut) Oil Blends and applications as cutting fluid. Agric Sci Res J. 2019;9(4):35–41.
Nyakuma BB. Thermogravimetric and kinetic analysis of Melon (Citrullus colocynthis L.) seed husk using the distributed activation energy model. Environ Clim Technol. 2015;15(1):77–89.
Milenković DD, Bojić AL, Veljković VB. Ultrasound-assisted adsorption of 4-dodecylbenzene sulfonate from aqueous solutions by corn cob activated carbon. Ultrason Sonochem. 2013;20(3):955–62.
Nicoleta Matei, Scarpete D. Treatment of Wastewater by Ultrasound Intensity and Frequency Effect : A Review. ARPN J Sci Technol. 2015;5(11):591–7.
Parthasarathy S, Mohammed RR, Fong CM, Gomes RL, Manickam S. A novel hybrid approach of activated carbon and ultrasound cavitation for the intensification of palm oil mill effluent (POME) polishing. J Clean Prod. 2016;112(January):1218–26.
Entezari MH, Soltani T. Simultaneous removal of copper and lead ions from a binary solution by sono-sorption process. J Hazard Mater. 2008;160(1):88–93.
Odoemelam SA, Onwu FK, Uchechukwu SC, Chinedu MA. Adsorption Isotherm Studies of Cd (ll) and Pb (ll) Ions from Aqueous Solutions by Bamboo-Based Activated Charcoal and Bamboo Dust. 2015;5(3):253–69.
Raya I, Zakir M. The Adsorption of Pb (II) Ions on Activated Carbon from Rice Husk , Irradiated by Ultrasonic Waves : Kinetic and Thermodynamics Studies. J Nat Sci Res. 2014;4(2):18–24.
Sonochemistry U, Milenkovi DD, Veljkovi VB. Ultrasound-assisted adsorption of copper (II) ions on hazelnut shell activated carbon. 2013;(October 2015).

Babarinde A, Omisore GO, Oyebamiji Babalola J. Kinetic, isothermal and thermodynamic parameters for the biosorption of Ni(II), Cr(III), and Co(II) onto Melon (Citrillus lanatus) seed husk. Ijcbs [Internet]. 2014;6:18–33. Available from: www.iscientific.org/Journal.html

Armbruster MH, Austin JB. The Adsorption of Gases on Plane Surfaces of Mica. J Am Chem Soc. 1938;60(2):467–75.

Wang B, Gao B, Zimmerman AR, Lee X. Impregnation of multiwall carbon nanotubes in alginate beads dramatically enhances their adsorptive ability to aqueous methylene blue. Chem Eng Res Des [Internet]. 2018;133:235–42. Available from: https://doi.org/10.1016/j.cherd.2018.03.026

Chen X. Modeling of experimental adsorption isotherm data. Inf. 2015;6(1):14–22.

Cheng S, Zhang L, Xia H, Peng J, Shu J, Li C, et al. Adsorption behavior of methylene blue onto waste-derived adsorbent and exhaust gases recycling. RSC Adv [Internet]. 2017;7(44):27331–41. Available from: http://dx.doi.org/10.1039/C7RA01482A

Aurich A, Hofmann J, Oltrogge R, Wecks M, Gläser R, Blömer L, et al. Improved Isolation of Microbiologically Produced (2R,3S)-Isocitric Acid by Adsorption on Activated Carbon and Recovery with Methanol. Org Process Res Dev. 2017;21(6):866–70.

Zhang X, Wang X, Chen Z. A novel nanocomposite as an efficient adsorbent for the rapid adsorption of Ni(II) from aqueous solution. Materials (Basel). 2017;10(10):1–22.

Ait Ahsaine H, Zbair M, Anfar Z, Naciri Y, El haouti R, El Alem N, et al. Cationic dyes adsorption onto high surface area 'almond shell' activated carbon: Kinetics, equilibrium isotherms and surface statistical modeling. Mater Today Chem [Internet]. 2018;8:121–32. Available from: https://doi.org/10.1016/j.mtchem.2018.03.004

Mechi N, Ben Khemis I, Dotto GL, Franco D, Sellaoui L, Ben Lamine A. Investigation of the adsorption mechanism of methylene blue (MB) on Cortaderia selloana flower spikes (FSs) and on Cortaderia selloana flower spikes derived carbon fibers (CFs). J Mol Liq [Internet]. 2019;280:268–73. Available from: https://doi.org/10.1016/j.molliq.2019.02.024

Ozbay N, Yargic AS. Comparison of Surface and Structural Properties of Carbonaceous Materials Prepared by Chemical Activation of Tomato Paste Waste: The Effects of Activator Type and Impregnation Ratio. J Appl Chem. 2016;2016:1–10.

Kumar A, Jena HM. Preparation and characterization of high surface area activated carbon from Fox nut (Euryale ferox) shell by chemical activation with H3PO4. Results Phys [Internet]. 2016;6:651–8. Available from: http://dx.doi.org/10.1016/j.rinp.2016.09.012

Sharma YC, Uma. Optimization of parameters for adsorption of methylene blue on a low-cost activated carbon. J Chem Eng Data. 2010;55(1):435–9.

Auta M, Hameed BH. Preparation of waste tea activated carbon using potassium acetate as an activating agent for adsorption of Acid Blue 25 dye. Chem Eng J [Internet]. 2011;171(2):502–9. Available from: http://dx.doi.org/10.1016/j.cej.2011.04.017

Bakti AI, Gareso PL. Characterization of Active Carbon Prepared from Coconuts Shells using FTIR, XRD and SEM Techniques. J Ilm Pendidik Fis Al-Biruni. 2018;7(1):33–9.

Kwasi Opoku B, Isaac A, Akrofi Micheal A, Kwesi Bentum J, Paul Muyoma W. Characterization of Chemically Activated Carbons Produced from Coconut and Palm Kernel Shells Using SEM and FTIR Analyses. Am J Appl Chem. 2021;9(3):90.

Hamdaoui O, Naffrechoux E. Adsorption kinetics of 4-chlorophenol onto granular activated carbon in the presence of high frequency ultrasound. Ultrason Sonochem. 2009;16(1):15–22.

Mouni L, Belkhiri L, Bollinger JC, Bouzaza A, Assadi A, Tirri A, et al. Removal of Methylene Blue from aqueous solutions by adsorption on Kaolin: Kinetic and equilibrium studies. Appl Clay Sci. 2018;153(November 2017):38–45.

Tang YZ, Gin KYH, Aziz MA. The relationship between pH and heavy metal ion sorption by algal biomass. Adsorpt Sci Technol. 2003;21(6):525–38.